# One-dimensional Model of an Optimal Ejector and Parametric Study of Ejector Efficiency

*Ronan K. McGovern[a], Kartik V. Bulusu[b], Mohammed A. Antar[c] and John H. Lienhard V[d]*

[a] *Massachusetts Institute of Technology, Cambridge, MA, U.S.A., mcgov@mit.edu*
[b] *The George Washington University, Washington D.C., U.S.A., bulusu@gwmail.gwu.edu*
[c] *King Fahd University of Petroleum and Minerals, Dhahran, Saudi Arabia, antar@kfupm.edu.sa*
[d] *Massachusetts Institute of Technology, Cambridge, MA, U.S.A., lienhard@mit.edu*

**Abstract:**

Significant numerical and experimental analyses have been devoted to understanding the variety of flow regimes present in steady flow ejectors. Certain regimes are more conducive to achieving high performance (i.e. high entrainment ratios). In particular, the entrainment ratio is seen to be highest when the entrained fluid reaches a choked condition in the mixing region. In addition, the expansion regime of the motive nozzle (under-, perfectly- or over-expanded) appears to influence performance. In this paper, we propose a method to model an ejector of optimal geometry, designed for a favorable flow regime. Then, rather than focusing upon the maximization of efficiency, we seek operational conditions that maximise ejector efficiency, specifically the reversible entrainment ratio efficiency. Ejector efficiency is found to be highest at low compression ratios and at low driving pressure ratios. However, at lower compression ratios, the optimal area of the mixing chamber becomes large relative to the motive nozzle throat area.

# 1. Introduction

Ejectors are supersonic flow induction devices employed for the generation of a vacuum for compressing a fluid. Figure 1 shows a straight throat ejector. High pressure motive fluid enters a converging diverging nozzle and is accelerated to a supersonic Mach number. The pressure at section NE is below that of the entrained fluid at its inlet. Consequently, the entrained fluid is drawn into the ejector. The motive and entrained fluids mix between sections NE and U and the uniform mixture is diffused to reach the discharge pressure.
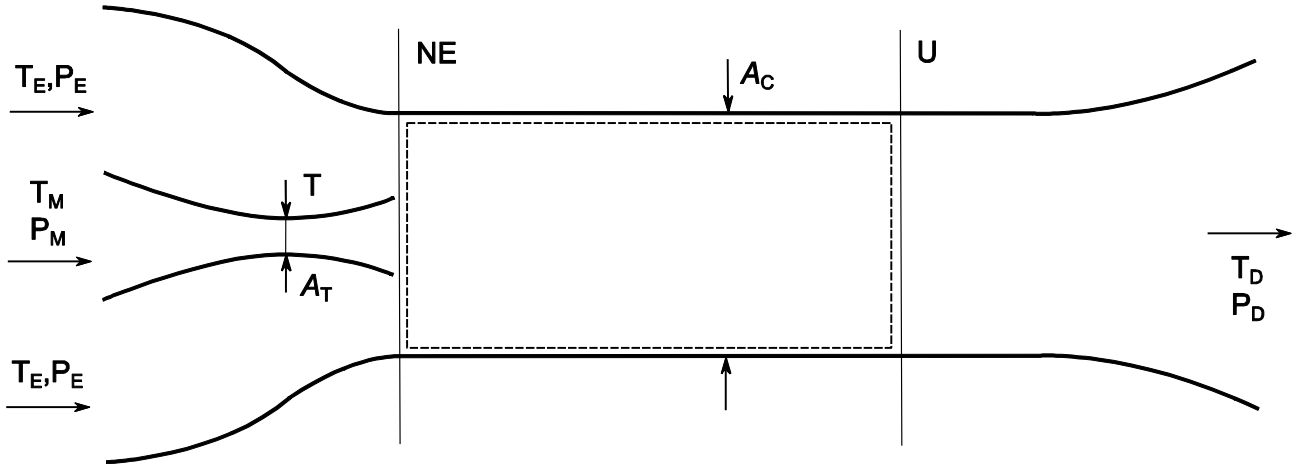


*Fig. 1. Schematic diagram of a straight throat ejector*

One common ejector application is the withdrawal of non-condensible gases from steam condensers. Other applications employ ejectors to compress a working fluid, such as vapor-compression refrigeration and vapor compression multi-pressure humidification-dehumidification desalination [3]. The operating conditions of an ejector in vacuum generation and compression applications differ significantly. When generating a vacuum, the compression ratio of the ejector, $P_D/P_E$, is very high whilst the ratio of the mass flow rate of entrained to motive fluid (known as the entrainment ratio) is very high. In compression applications, the compression ratio is low, whilst the entrainment ratio is high. The compression ratios also differ between compression applications. For example, Huang et al. [1] performed experiments on a refrigeration system using R141b. For an evaporator temperature of 8°C and a condenser temperature ranging from 28°C to 42.1°C, the compression ratio of the ejector varied from 2.2 to 3.6. Kamali et al. [2] optimised the design of a seven effect thermal vapour compression multi-effect distillation system with a condenser temperature of 45°C and a first effect temperature of 69°C, corresponding to a compression ratio of 3.1. Narayan et al. [3] optimised an ejector driven humidification dehumidification desalination system and found that the optimal compression ratio lies near 1.2.

For compression applications, the ejector efficiency is of significant importance as it dictates the energy input (or more correctly the exergy input) required to drive the ejector. One means of quantifying ejector performance, suggested by Elrod [4] and analysed in detail by McGovern et al. [5], is the reversible entrainment ratio efficiency, or $\eta_{RER}$. This efficiency compares the entrainment ratio of a real ejector to a reversible process with the same inlet fluid states and the same discharged pressure:

$$\eta_{RER} = \frac{ER}{RER} \qquad (1)$$

When designing an ejector, we could look for more than just a high value of entrainment ratio for fixed inlet conditions and a fixed discharge. Importantly, the entrainment ratio alone is not an indication of the quality of design or the performance of an ejector. We can ask what ejector

geometry *and* what operating conditions are conducive to the highest ejector efficiency. This is the objective of the present work. In Section 2, we identify the flow regimes possible in steady flow ejectors that are most conducive to high efficiency. In Section 3, we discuss how an ejector of optimal geometry may be modelled using 1 dimensional theory. In Section 4, using fluid inlet conditions and ejector discharge pressure as parameters, we identify the operating conditions conducive to the highest values of efficiency. In summary, by focusing upon efficiency rather than solely the entrainment ratio we provide a new insight to optimising ejector design.

# 2. Regimes of Ejector Operation

One crucial consideration in the analysis and design of ejectors is the variety of flow regimes that are possible, depending on operating conditions and the ejector geometry. In order to design for maximum ejector efficiency one should be able to identify favorable flow regimes. To understand the flow regimes of an ejector we can describe the entrainment ratio in terms of the inlet fluid conditions, the discharged pressure, the motive fluid nozzle throat area and the mixing chamber area.

$$ER = f(P_M, T_M, P_E, T_E, P_D, A_T, A_C) \qquad (2)$$

First, we would like to explain the effect of the operating conditions upon an ejector of fixed geometry and second, the effect of the ejector geometry upon the entrainment ratio of an ejector with fixed operating conditions. This is done by considering experimental and numerical analyses present in literature.

## 2.1 Flow regimes within an ejector of fixed geometry

The explanation of flow regimes for a fixed ejector geometry is common in literature and revolves around the concept of critical back pressure, $P_D*$. A clear description of the critical pressure is provided by Bartosiewicz et al. and Huang et al. [6, 20] using experimental data and by Sriveerakul et al. [7] using a CFD analysis. The motive fluid throat area, the chamber area and the inlet motive and entrained fluid states at the inlet to the ejector are fixed. We may now describe three distinct regimes:

1. Reversed flow region – $P_D$ is to the right of point A on the *x* axis of Fig. 2 and the discharged pressure is too high to allow entrainment. Flow through the converging diverging nozzle is overexpanded, resulting in compression shocks (see Bartosiewicz [6]). Motive fluid partially flows back through the entrained fluid inlet.

2. Unchoked entrainment – The discharged pressure drops to point A in Fig. 2, causing the compression shocks at the exit of the motive fluid nozzle to weaken, allowing the pressure at NE to drop and provoke entrainment.

3. Critical operation – The discharged pressure reaches $P_D*$, allowing a decrease in pressure upstream and causing the entrained flow to be accelerated to sonic speed within the mixing region.

4. Choked Flow – For values of $P_D$ below $P_D*$ the entrainment ratio remains constant. The motive fluid is choked at the motive fluid nozzle throat and the entrained flow remains choked in the mixing region.

The important message to take from these analyses is that the entrained mass flow rate is constant as the discharge pressure drops below critical. Since the entrained fluid pressure is held constant at the inlet this can only mean that the effective cross-sectional area at which choking occurs in the mixing region must be constant for fixed inlet conditions and ejector geometry, as concluded by Munday and Bagster [8].
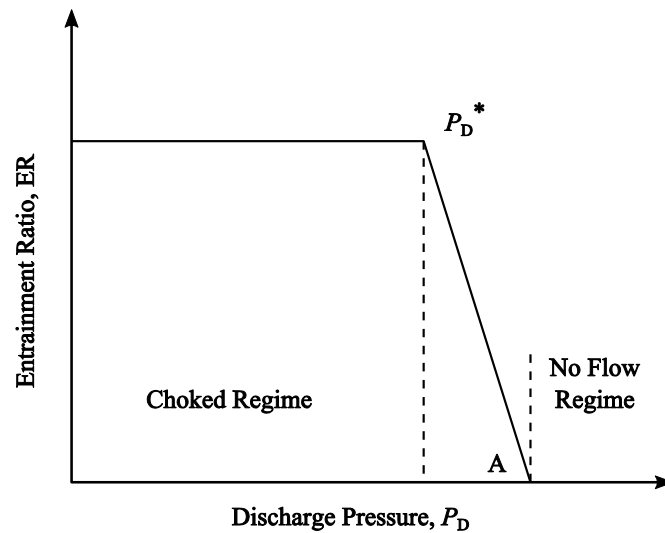
*Fig. 2. Evolution of the entrainment ratio with discharge pressure*

## 2.2 Flow regimes within an ejector with fixed operating conditions

Less common in literature is an intuitive explanation of the effect of ejector geometry upon the entrainment ratio. Nahdi et al. [9] and Lu et al. [10] draw important conclusions in this regard. By considering fixed inlet fluid states and a fixed discharged pressure we may identify three regimes which depend upon ejector geometry.

1. Overexpanded Flow – We consider operating conditions such that the motive and entrained fluids are choked at the motive nozzle throat and in the mixing chamber, respectively. The ratio of chamber to motive nozzle throat area, $\varphi$, is small, such that the motive nozzle is overexpanded.

2. Perfectly Expanded Flow – The value of $\varphi$ is reduced causing a higher value of ER. The pressure at cross section U in Fig. 1 drops, as does the pressure upstream of U. The compression shocks downstream of the motive fluid nozzle weaken until they cease to exist when the nozzle is perfectly expanded. The effective flow area of the entrained fluid increases (since $\varphi$ increases) and the entrainment ratio increases. Nahdi et al. refer to $\varphi$ at this point as the optimal area ratio for a given set of inlet conditions and discharged pressure. The entrainment ratio is maximum, the static pressures of the motive and entrained fluid are equal at section NE in Fig. 1 and the motive nozzle is perfectly expanded.

3. Underexpanded Flow – The value of $\varphi$ is reduced below optimal, causing a decrease in entrainment. The underexpanded motive jet spreads at the exit of the motive nozzle, restricting the flow area of the entrained fluid. The flow structure takes the form of Fig. 3.
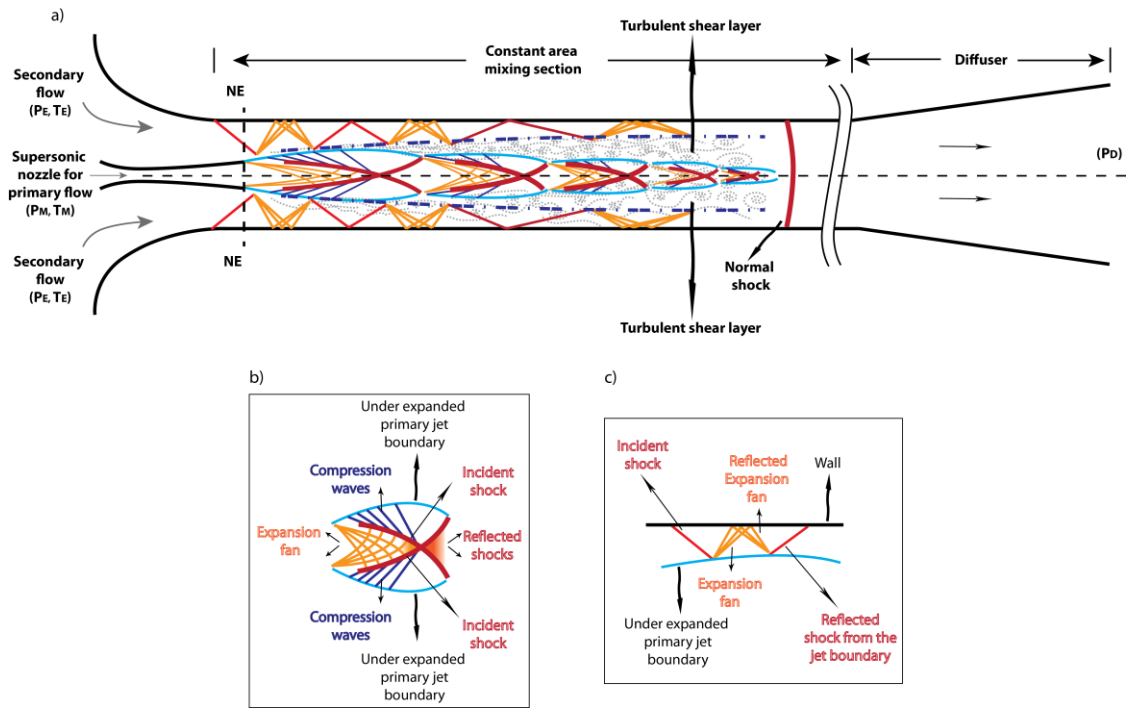
*Fig. 3. Representation of the flow structure in an ejector with an underexpanded motive fluid nozzle and choked entrained flow*

Using experimental results, Nahdi et al. [9] recognise that the entrainment ratio of an ejector is maximised when the primary nozzle is perfectly expanded and the entrained fluid reaches a choked condition. They identify, for a working fluid of R11, the area ratio which maximises the ER, as a function of ejector compression ratio, $P_D/P_E$, and driving pressure ratio, $P_M/P_D$.

# 3. One Dimensional Model of an Optimal Ejector

Using this knowledge we can build a one-dimensional ejector model that captures the performance of an optimal ejector. Coupled with the definition for efficiency (Section 1), this model can be used to identify the ejector operating conditions conducive to high efficiency (Section 4).

Nahdi et al. [9] identified the flow regime that maximised the ER for fixed conditions of operation. Since the reversible entrainment ratio is constant for fixed conditions of operation [4, 5], the flow regime that maximizes the ER must also maximize the reversible entrainment ratio efficiency. Consequently, the purpose of this section is to model an ejector operating in this optimal flow regime. Using this knowledge we can build a one-dimensional ejector model that captures the performance of an optimal ejector. Coupled with the definition for efficiency (Section 1), this model can be used to identify the ejector operating conditions conducive to high efficiency (Section 4). To simplify the interpretation of results, an ideal gas ejector is modelled, with constant values of specific heats.

## 3.1 Nozzle Region

We begin by considering flow from the motive and entrained fluid inlets to the cross section NE in Fig. 1. The inlet fluid pressures and temperatures are fixed, $P_M$, $P_E$, $T_M$, $T_E$. According to Section 3, the motive fluid nozzle is perfectly expanded, meaning that the static pressures of the motive and entrained streams are equal at NE. In addition, the entrained flow is choked at section NE, *i.e.* the Mach number is unity, such that further decreases in the downstream pressure cannot induce a higher mass flow rate. Considering the motive and entrained flows both to be isentropic and

adiabatic, we may solve for the entrained fluid pressure and temperature at the nozzle exit, and then for the motive fluid Mach number and the motive fluid temperature at NE.

$$\frac{T_E}{T_{NE,E}} = 1 + \frac{\gamma - 1}{2} \tag{3}$$

$$\frac{P_E}{P_{NE,E}} = (1 + \frac{\gamma - 1}{2})^{\frac{\gamma}{\gamma - 1}} \tag{4}$$

$$\frac{P_M}{P_{NE,M}} = (1 + \frac{\gamma - 1}{2} M_{NE,M}{}^2)^{\frac{\gamma}{\gamma - 1}} \tag{5}$$

$$\frac{T_M}{T_{NE,M}} = 1 + \frac{\gamma - 1}{2} M_{NE,M}{}^2 \tag{6}$$

In order to fix the capacity of the ejector, we fix the motive fluid throat area, $A_T$. This allows the mass flow of the motive fluid to be calculated:

$$\dot{m}_M = \frac{\sqrt{\gamma} A_T P_M}{\sqrt{RT_M}} (1 + \frac{\gamma - 1}{2})^{-\frac{\gamma + 1}{2(\gamma - 1)}} \tag{7}$$

At this point, the mass flow rate (and the flow area at NE) of the entrained fluid is yet to be determined. The modelling until this point is the same as Khoury et al. [11], although their work does not allude to the motive nozzle being perfectly expanded to justify the uniformity of pressure across NE. In the present analysis, the motive nozzle exit is located at the entrance to the mixing region (Fig. 1). In many experimental configurations, the nozzle exit is upstream of the constant area region. Zhu et al. [12] provide a detailed analysis of the influence of the axial position of the nozzle exit upon entrainment ratio.

## 3.2 Mixing Region

In the constant area mixing region, the mass, momentum, and energy conservation equations are applied between sections NE and U of Fig. 1. The fluid properties and velocity are taken to be uniform over the entrained flow area and motive flow area at NE and over the total flow area at U. Frictional forces on the fluid due to the no slip condition at the wall are assumed to be negligible.

$$\dot{m}_M + \dot{m}_E = \dot{m}_U \tag{8}$$

$$P_{NE} A_{NE} + \dot{m}_M V_{NE,M} + \dot{m}_E V_{NE,E} = P_U A_U + \dot{m}_U V_U \tag{9}$$

$$\dot{m}_M c_p T_{NE,M} + \dot{m}_E c_p T_{NE,E} = \dot{m}_U c_p T_U \tag{10}$$

In addition, there is a relationship between the mixing chamber area and the flow areas at the exit of the motive nozzle.

$$A_{NE} = A_{NE,M} + A_{NE,E} = A_U \tag{11}$$

A number of these assumptions merit further discussion. The mixing process within an ejector is characterised by highly irreversible oblique and sometimes normal shocks coupled with dissipative processes within the shear layer between the motive and entrained fluids. Entropy generation within this region is driven by pressure, velocity and temperature differences, in axial and radial directions.

By employing a control volume approach, we are overlooking the details of the mixing process. Instead, by essentially varying the ratio of pressure, velocity and temperature, the motive and entrained fluids at NE and the pressure ratio between sections NE and U, we are essentially altering the scale of the disequilibria responsible for entropy generation. Examples of detailed experimental visualisations of internal flow structures are provided by Desevaux et al. [14] and Dvorak et al. [19], whilst numerical visualisations are provided by Desevaux et al. [13], Hemidi et al. [15], Bartosiewicz et al. [6] and Sriveerakul et al. [7].

By assuming properties and velocity to be uniform at section U in Fig. 1, we intend the ratio of the mixing chamber length to diameter to be sufficiently large for the motive fluid core and the entrained fluid annulus to have mixed very well. The consequence of incomplete mixing is inadequate pressure recovery and compression within the diffuser. The axial length of the mixing section is dependent on the rate of mixing between the two streams. The higher the rate of mixing the greater would be the transverse spread (or growth) of the turbulent shear layer leading to a shorter axial length of the mixing region. Li et al. [16] indicated that the optimum length varies greatly with the operation conditions. In numerical studies, one way to determine the appropriate mixing length is by employing a numerical die tracer, as suggested by Bartosiewicz et al. [6]. Sriveerakul et al. [7] also points out that as the mixing chamber is elongated, total pressure losses due to shear stress at the wall increase, implying that there is an optimal length of the mixing region.

## 3.3 Diffuser

Since the fluid velocity is considered to be uniform at cross section U in Fig. 1, the diffuser is modelled as isentropic.

$$\frac{T_D}{T_U} = 1 + \frac{\gamma - 1}{2} M_U{}^2 \qquad (12)$$

$$\frac{P_D}{P_U} = (1 + \frac{\gamma - 1}{2} M_U{}^2)^{\frac{\gamma}{\gamma - 1}} \qquad (13)$$

In practice, the performance of the diffuser depends largely upon the completeness of mixing in the constant area section. Diffuser efficiency was reported by Varga et al. [17] to be within the range 0.5 to 0.9 depending on both temperature and area ratio. For an ejector of fixed mixing chamber length, the diffuser efficiency is a function of the back pressure. As back pressure increases, normal or oblique shocks will be pushed back into the mixing section, resulting in a more uniform flow at cross section U and consequently improved diffuser performance. This is clearly illustrated by Sriveerakul et al. [7].

## 3.4 Solution of Equations

Given the following relations for mass flow rate, Mach number and the speed of sound in an ideal gas, the set of equations provided above are closed and may be solved.

$$\dot{m} = \rho A V \qquad (14)$$

$$M = \frac{V}{c} \qquad (15)$$

$$c = \sqrt{\gamma R T} \qquad (16)$$

The equations are solved iteratively using the non-linear equation solver provided by Engineering Equation Solver [18] subject to the restriction that the Mach number obtained at cross section U

must be subsonic. For compression applications, the conditions of the fluid obtained at the diffuser exit should be as close as possible to stagnation (zero velocity). Consequently, the flow must be subsonic at the diffuser exit, and preferably within the entire diffuser. For a set of operational conditions (inlet fluid states and discharge pressure), we may calculate the following key variables:

1. The ejector area ratio of $A_C/A_T$
2. The entrainment ratio, ER

# 4. Results

Given the model of an optimal ejector presented in Section 3, we now seek the conditions of operation that maximize ejector efficiency. We begin by considering the variation in ejector efficiency and area ratio with the compression ratio in Fig. 4. As the compression ratio decreases, the entrainment ratio of the optimal ejector increases at a faster rate than the reversible entrainment ratio, resulting in improved efficiency. Meanwhile, as the compression ratio drops, the optimal area ratio of the mixing chamber to the ejector throat increases to accommodate a greater flow rate of entrained fluid.
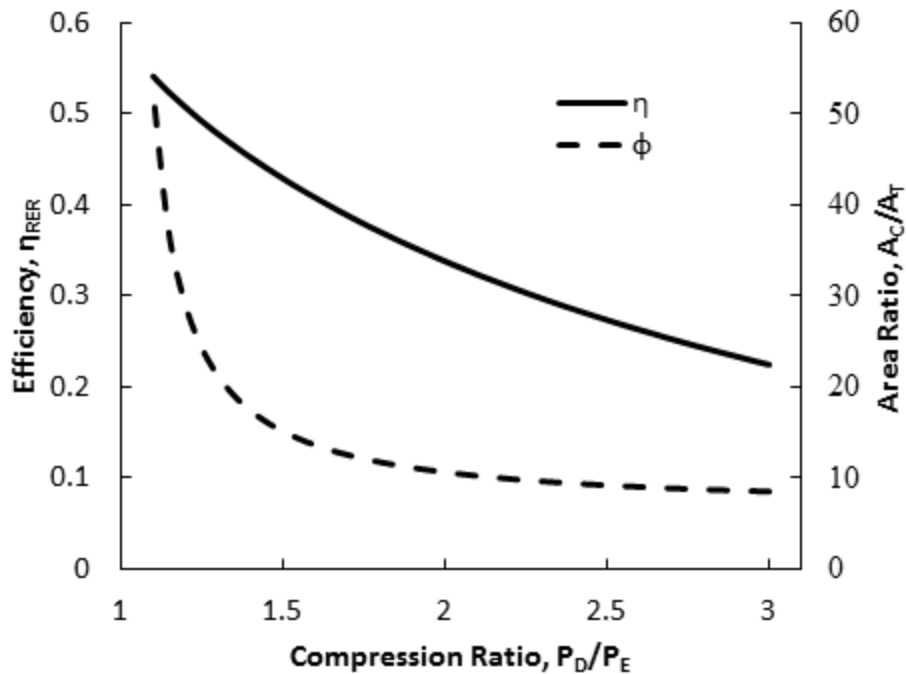


*Fig. 4. Efficiency and area ratio for a driving pressure ratio of $P_M/P_D=5$ and an inlet temperature ratio of $T_M/T_E=1$*

Figure 5 illustrates the effect of the driving pressure ratio upon ejector efficiency and area ratio. Ejector efficiency is less sensitive to the driving pressure ratio of the ejector than the compression ratio. As the driving pressure ratio increases, the area ratio of the ejector also increases, resulting in an ejector that is larger in size.
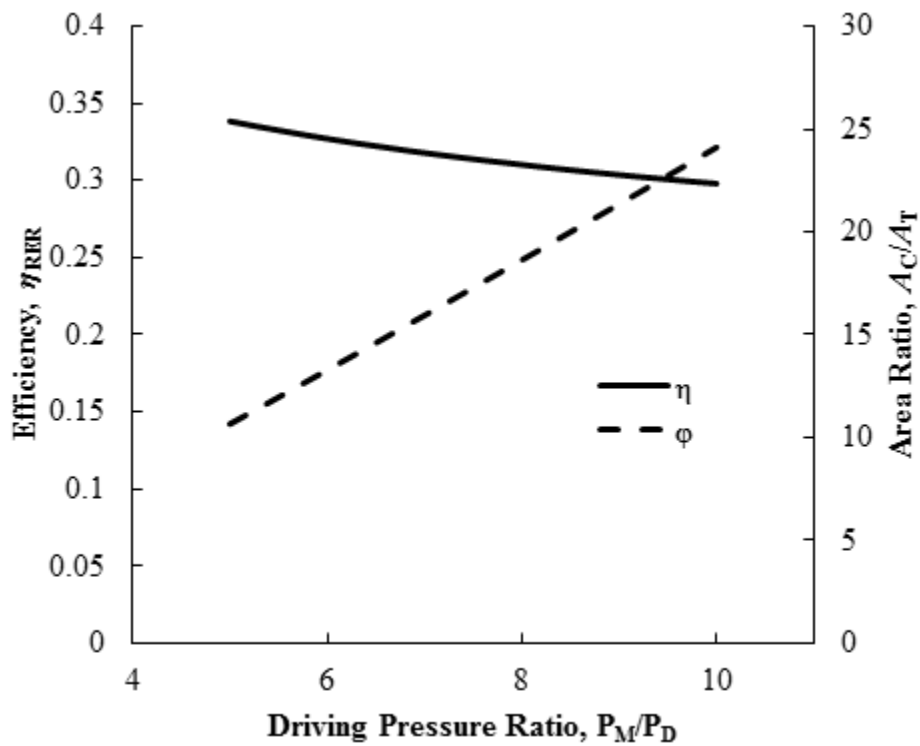


Fig. 5. Efficiency and area ratio for a compression ratio of $P_D/P_E=2$ and an inlet temperature ratio of $T_M/T_E=1$

Finally, we consider the effect of the inlet temperature ratio. In Fig. 5, the efficiency of the ejector reaches a maximum at an inlet temperature ratio just above unity. This is the point where the temperature difference between the motive and entrained streams at the nozzle exit are minimum. Also, the ejector area ratio is insensitive to the inlet temperature ratio.
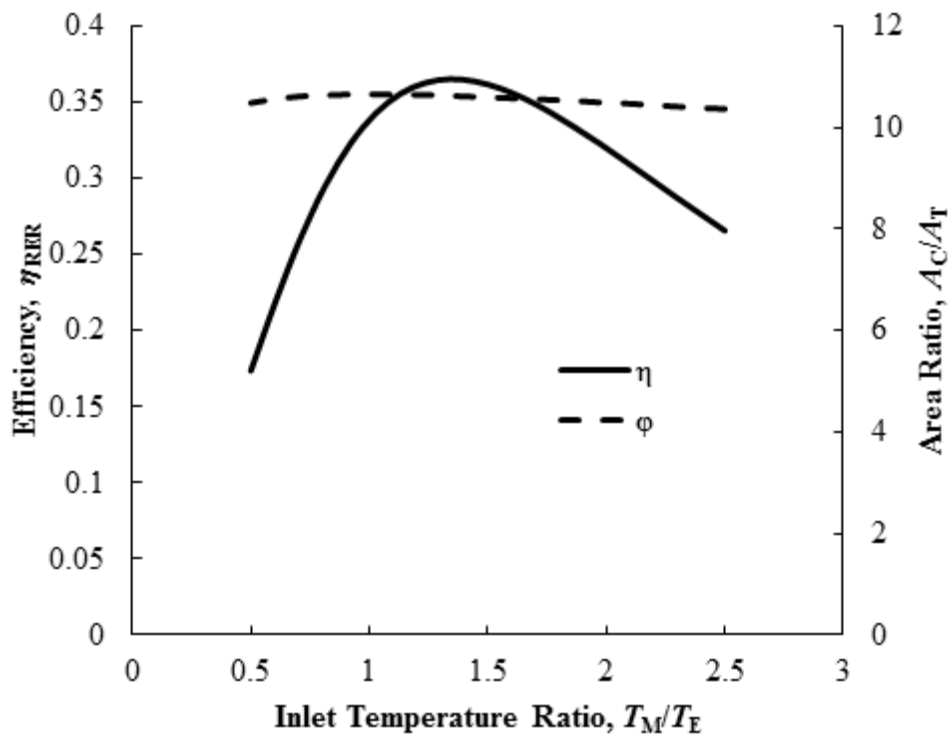


*Fig. 6. Efficiency and area ratio for a driving pressure ratio of $P_M/P_D=5$ and an inlet temperature ratio of $T_D/T_E=2$*

## 5. Conclusions

Using a simple model of an optimal ejector, a parametric study has been performed to identify operating conditions conducive to high ejector efficiency. This optimal ejector is designed such that the motive fluid nozzle is perfectly expanded and the entrained fluid is choked at the entrance to the constant area mixing section. The following is concluded from the parametric study:

- The efficiency of an ideal gas ejector is highest when design for conditions of low compression ratio and low driving pressure ratio.
- At low compression ratios the area ratio of the mixing section to the motive nozzle throat increases, indicating that the required size of the ejector increases.
- As the driving pressure ratio increases, the required size of the ejector increases
- An optimal inlet temperature ratio of the inlet fluids appears to exist for fixed inlet and discharge pressures, although the ejector area ratio appears insensitive to the inlet temperature ratio

## Acknowledgments

# Nomenclature

**Letter Symbols**

$A$   area, m$^2$

$c$   speed of sound, m/s

ER      entrainment ratio, dimensionless

$\dot{m}$ mass flow rate, kg/s

$M$ speed of sound, dimensionless

$P$ pressure, Pa

$R$ ideal gas constant, J/kg K

RER    reversible entrainment ratio, dimensionless

$T$ temperature, K

**Greek symbols**

$\eta$   reversible entrainment ratio efficiency, dimensionless

$\gamma$   ratio of specific heats, dimensionless

$\varphi$   Ratio of mixing chamber area to motive nozzle throat area

**Subscripts**

C  mixing chamber area

D  discharge

E  entrained fluid

M  motive fluid

NE      motive nozzle exit

T  motive nozzle throat

U  uniform flow cross section

**Abbreviations**

ER      entrainment ratio

RER    reversible entrainment ratio

# References

[1] Huang B.J., Chang J.M., Wang C.P., Petrenko V.A., A 1-D analysis of ejector performance. International Journal of Refrigeration 1999;22:354–364.

[2] Kamali R.K., Abbassi A., Sadough Vanini S.A., Saffar Avval M., Thermodynamic design and parametric study of MED-TVC. Desalination 2008;222:596-604

[3] Narayan G.P. McGovern R.K., Zubair S.M., Lienhard V J.H., High-temperature-steam-driven, varied-pressure, humidification-dehumidification system coupled with reverse osmosis for energy-efficient seawater desalination. Energy 2012;27(1):482‑493.

[4] Elrod H.G., The Theory of Ejectors. Journal of Applied Mechanics 1945;12:A170-A174

[5] McGovern R.K., Narayan G.P., Zubair S.M., Lienhard V J. H., Analysis of reversible ejectors and definition of an ejector efficiency. International Journal of Thermal Sciences 2012;54:153-166.

[6] Bartosiewicz Y., Aidoun Z., Desevaux P, Mercadier Y., Numerical and experimental investigations on supersonic ejectors, International Journal of Heat and Fluid Flow. 2005; 26:56–70.

[7] Sriveerakul K. , Aphornratana S., Chunnanond K., Performance predict tion o fsteam ejector using computational fluid dynamics: Part 2: Flow structure of a steam ejector influenced by operating pressure and geometries, International Journal of Thermal Sciences 2007;46:823–33.

[8] Munday J.T., Bagster D.F., A New Ejector Theory Applied to Steam Jet Refrigeration. Industrial & Engineering Chemistry Process Design and Development 1977;16(4):442-449.

[9] Nahdi E., Champoussin J.C., Hostache G., Cheron J. Optimal geometric parameters of a cooling ejector-compressor. Revue International du Froid 1993;16(1):67-72

[10] Lu T.C., Champoussin J.C., Nahdi E., Optimal performance and use of an ejector cycle refrigeration system. 17$^{eme}$ Congres International du Froid AARAC/IIR; 1987; Wien:969- 974.

[11] Khoury F., Heyman M., Resnick W., Performance Characteristics of Self-Entrainment Ejectors. ILEC Process Design and Development 1967;6(3):331-340.

[12] Zhu Y., Cai W., Wen C., Li Y., Simplified ejector model for control and optimization, Energy Conversion and Management.2008; 49:1424-32.

[13] Desevaux P., Marynowski T., Khan M., CFD prediction of supersonic ejector performance, International Journal of Turbo and Jet Engines. 2006; 23:173-81.

[14] Desevaux P., A method for visualizing the mixing zone between two co-axial flows in an ejector, Optics and Lasers in Engineering. 2001;35:317–23.

[15] Hemidi A., Henry F., Leclaire S., Seynhaeve J.M., Bartosiewicz Y., CFD Analysis of a Supersonic Air Ejector. Part I: Experimental Validation of Single-Phase and Two-Phase Operation. Applied Thermal Engineering 2008. Applied Thermal Engineering 2009;29(8-9):1523‑1531.

[16] Li C., Li Y., Wang L., Configuration dependence and optimization of the entrainment performance for gas-gas and gas-liquid ejectors. ATE In press.

[17] Varga S., Oleviera A. C., Diaconu B., Numerical Assessment of Steam Ejector Efficiencies using CFD, Internatinal Journal of Refrigeration. 2009;32:1203-11.

[18] Klein S.A., Engineering Equation Solver, Academic Professional, Version 8, 2009; Madison, WI; www.fchart.com.

[19] Dvorak V., Safarik P., Supersonic Flow Structure in the Entrance Part of a Mixing Chamber of 2D Model Ejector, Journal of Thermal Science. 2003;12(4):344-349.

[20] Huang B. J., Jiang C. B.., Hu F. L., Ejector Performance Characteristics and Design Analysis of Jet Refrigeration System, Journal of Engineering for Gas Turbines and Power, Transactions of the ASME. 1985; 107(3):792-803.